AIP Advances

GdN/SmN superlattices; influence of a Zeeman/exchange conflict

Cite as: AIP Advances **11**, 015348 (2021); https://doi.org/10.1063/9.0000099
Submitted: 14 October 2020 . Accepted: 05 January 2021 . Published Online: 28 January 2021

E.-M. Anton, W. F. Holmes-Hewett, J. F. McNulty, F. Natali, F. Bramley, Y. Choi, D. Haskel, B. J. Ruck, and H. J. Trodahl

GdN/SmN superlattices; influence of a Zeeman/exchange conflict

Cite as: AIP Advances 11, 015348 (2021); doi: 10.1063/9.0000099
Presented: 2 November 2020 • Submitted: 14 October 2020 •
Accepted: 5 January 2021 • Published Online: 28 January 2021

E.-M. Anton,[1,a] W. F. Holmes-Hewett,[1] J. F. McNulty,[1] F. Natali,[1] F. Bramley,[1] Y. Choi,[2] D. Haskel,[2] B. J. Ruck,[1] and H. J. Trodahl[1]

AFFILIATIONS

[1]The MacDiarmid Institute for Advanced Materials and Nanotechnology, School of Chemical and Physical Sciences, Victoria University of Wellington, P.O. Box 600, Wellington 6140, New Zealand
[2]Advanced Photon Source, Argonne National Laboratory, Argonne, Illinois 60439, USA

Note: This paper was presented at the 65th Annual Conference on Magnetism and Magnetic Materials.
[a]**Author to whom correspondence should be addressed:** eva.anton@vuw.ac.nz

ABSTRACT

GdN and SmN are two of the lanthanide nitrides, most of which are intrinsic ferromagnetic semiconductors. Superlattices comprising the pair offer a unique opportunity to investigate heterojunctions that feature simultaneous conductivity and magnetic interface influences. Here we report an investigation of these influences, using magnetisation and X-ray magnetic circular dichroism for magnetic effects, and magnetoresistance and Hall effect studies of their electrical conductance. Magnetic data show clear signatures of a conflicting Zeeman vs. interfacial exchange and the magnetic disruption that results, while resistivity and Hall measurements show conduction in both GdN and SmN.

I. INTRODUCTION

Semiconductor heterojunctions have become some of the most important structures within electronics technology, opening the door to confined electron gases, tunneling structures, high electron-mobility transistors, quantum well lasers and much more.[1–4] Ferromagnetic hetero-interfaces have likewise driven technological advances: giant magnetoresistance and tunneling magnetoresistance random access memory (MRAM) to mention just two.[5] However, combined semiconductor/ferromagnetic hetero-interfaces, comprising both magnetic and electronic-state control, have until recently been unrealised, a result of the relative paucity of intrinsic ferromagnetic semiconductors.[6]

Within this scenario the rare-earth nitrides, LN (L a lanthanide element) can offer new opportunities, for they harbour many such intrinsic ferromagnetic semiconductors.[7] Their Curie temperatures lie well below room temperature with a maximum of about 70 K for GdN, ideally suited for low temperature applications like superconducting computers, which require memory devices operating at cryogenic temperatures. Here LNs have an advantage over metallic ferromagnets due to their strong spin-polarisation beneficial for devices based on magnetic tunnel junctions. The series comprises 14 epitaxy-compatible compounds with a very simple NaCl structure. The spin/orbit alignment and magnetic response vary widely across the series, driven by the strong spin–orbit interaction in the $4f$ shell of the lanthanides. An especially strong contrast is found between the magnetic properties of GdN and SmN,[8–11] the pair of LN on which the present study is focused.

GdN has served for decades as the prototypical LN, encouraged by the relative simplicity of the Gd^{3+} half-filled $4f$ shell and its Curie temperature, which at 50-70 K is the highest in the series.[8,12,13] The $4f$-shell configuration is $^8S_{7/2}$, with $L = 0$ and $J = S = 7/2$. As is expected for that configuration its magnetisation in the ferromagnetic phase corresponds to 7 μ_B per Gd^{3+} ion, and the spherically symmetric orbital wave function leads to a very small coercive field of ~0.01 T. A cubic anisotropy field of 0.1 T was reported in Khazen *et al.*,[14] though a uniaxial anisotropy field of 0.6 T was also reported and presumed due to lattice strain. GdN has an optical absorption onset at ~1 eV, in agreement with an LSDA+U band structure, which further shows it to have a ~0.45 eV indirect (Γ - X) band.[15,16] As for all the LN, thin films are doped n-type by nitrogen vacancies to typically ≥ 10^{20} cm^{-3} in as-prepared films, reducible to ~ 10^{16} cm^{-3} when co-doped with Mg.[17]

The $4f$ shell of Sm^{3+} adopts the $^6H_{5/2}$ configuration, with $J = S = 5/2$, $L = 5$. The strong spin–orbit interaction and weak crystal-field influence on the $4f$ shell then ensures that the magnetisation of ferromagnetic SmN is vanishingly small, corresponding to ~ 0.035 μ_B per Sm^{3+} ion.[9,18] X-ray magnetic circular dichroism (XMCD) and anomalous Hall effect measurements identify that it is the *orbital* component that dominates the net magnetic moment, so that the $4f$ *spin* magnetic moment in SmN is *antialigned* to an applied field.[10,19] Its magnetocrystalline anisotropy, though somewhat larger than that of GdN, is nonetheless small. However, the very weak Zeeman interaction in SmN requires a very large magnetic field to overcome even that weak anisotropy; it has a coercive field > 10 T at low temperature (≤ 5 K).[9,10,19]

A conflict develops at a GdN/SmN interface as a consequence of SmN's orbital dominance. In an applied field the Zeeman interaction tends to align the net magnetisation in the individual layers, while interface exchange between Gd-Sm favors their spin alignment.[10,11] The GdN layer's large spin-only magnetisation is held firmly parallel to an applied field, so the conflict is accommodated within the SmN layer, which develops an exchange spring such that it is only far from the interface that the SmN magnetisation aligns with the field.[11] The present paper reports magnetisation, XMCD and anomalous Hall effect studies of the conflict's influence on the magnetic alignment in GdN/SmN superlattices.

II. EXPERIMENTAL DETAILS

The superlattices used in the present study were grown in two ultra-high vacuum systems on MgO and Al_2O_3 substrates. Metallic Gd and Sm sources were evaporated in the presence of carefully purified nitrogen gas. As for most of the lanthanide metals, atomically clean Gd and Sm surfaces show the facility to break the N_2 triple bond, forming their nitrides without any activation of the gas.[7,20] Even when grown at room temperature, the films are usually strongly (111) textured.[21] For the present study we prepared first a series of superlattices as 12×(10 nm GdN/x nm SmN), x = 0, 1.5, 5, 7.5, 10, a series that facilitated an exploration of the complex exchange spring and the effective exchange between adjacent GdN layers. All these superlattices were grown in a Thermionics vacuum chamber on MgO(111) substrates held at 400°C during growth, with a nitrogen pressure of 3 ×10^{-4} mbar. A further superlattice, 6×(10 nm GdN/16 nm SmN) was grown in a Riber system on a c-plane Al_2O_3 substrate, which was held at 400°C during growth, with a nitrogen pressure of 4 ×10^{-5} mbar. The film was then investigated by magnetisation, XMCD, resistance and Hall effect measurements. The films were all grown under ≤ 10^{-4} mbar of nitrogen, which dopes them with ~ 10^{21} cm^{-3} electrons.[7,17] All were capped with AlN or GaN in order to prevent oxidization.

Magnetisation was measured with a Quantum Design MPMS SQUID magnetometer and magneto-transport studies were performed in the Van der Pauw geometry in a Quantum design PPMS. XMCD was performed on beamline 4-ID-D at the Advanced Photon Source at Argonne National Laboratory. Data was collected on the Gd and Sm L_2-edges using partial fluorescence yield, where saturation and self-absorption distort the spectra.[22] These distortions are however independent of the magnetic field, allowing for direct comparisons of the amplitudes of the spectra at different fields.

III. RESULTS AND DISCUSSION

A. Magnetisation and influence of GdN-SmN interface exchange interaction

We turn first to a disruption of the GdN-GdN exchange through the exchange-spring structure in an intervening SmN layer. Figure 1 displays the magnetic responses in an in-plane magnetic field of superlattices with 10 nm GdN layers separated by varying thicknesses of SmN. The data are all plotted as the magnetic moment per Gd ion, and are normalised to the GdN saturation magnetisation of 7 μ_B. The magnetisation of SmN is too small to affect the saturation magnetisation measured by SQUID in these superlattices.

The homogeneous GdN film, an end member of the superlattice series, follows the pattern often reported, with a coercive field of 0.01 T and reaching saturation at ~ 0.1 T.[7] In comparison, the superlattice with 1.5 nm SmN layers shows the same coercive field, though with a slower approach to saturation. The implication is that a 1.5 nm SmN layer does not fully block GdN/GdN exchange; the exchange spring in SmN does not impact on the alignment at the two interfaces. Exchange blocking is, however, accomplished by 5 nm of SmN, and thereafter the magnetic response changes little with increasing SmN thickness, supporting the loss of interface-exchange spin alignment across a few nm of SmN. The picture that emerges is that there is a penalty imposed by the need to align the Sm^{3+} *spin* magnetic moment near the interfaces, in the presence of a Zeeman interaction that would on its own *anti*-align the Sm spin moments relative to an applied field. Thus the measured net superlattice magnetisation for SmN thicknesses ≥ 5 nm corresponds to the magnetisation in isolated 10 nm thick GdN layers.

The magnetisation measurements above do not resolve the vanishingly small SmN-layer magnetisation. Thus to advance further we have exploited the element-specific character of XMCD at the Gd and Sm L edges. The $L_{2,3}$ edge represents transitions into the $5d$ shell, the conduction band, and thus the $L_{2,3}$-edge XMCD signal follows the $5d$ spin alignment. The strong f-d exchange interaction ensures that the $5d$ spin alignment follows also the dominating $4f$ alignment.

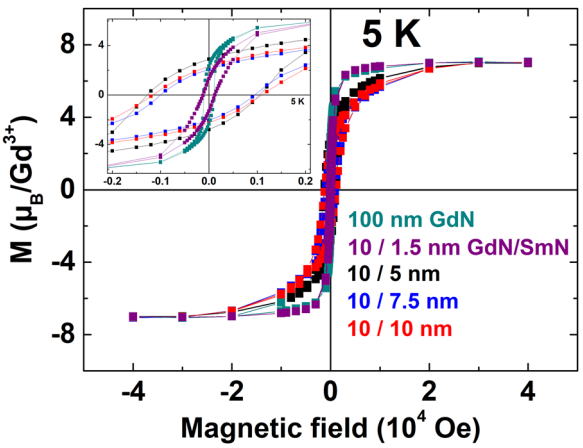

FIG. 1. (Colour online) In-plane magnetisation of a series of superlattices differing only in the thickness of the SmN layers. Both SmN and GdN are deep in the ferromagnetic state at 5 K.

Figure 2 shows XMCD spectra for both the Gd and Sm edges from a 6×[10 nm GdN/16 nm SmN] superlattice, collected at grazing incidence (70° from the normal). The data were collected at 2 K and with a magnetic field of 6 T, followed by a measurement in zero field. Looking first at the Gd data, one sees that the signal is almost twice as strong in 6 T than in the remanent magnetisation when the field is reduced to zero, in full agreement with the SQUID measurement of the hysteresis shown in the inset. The XMCD signal in Sm is of the same sign as in Gd, in direct opposition to the signal in bulk SmN,[10] indicating that in this superlattice the average spin alignment in the SmN layers is opposite to that in bulk SmN. Clearly the SmN layers in the superlattice carry an average spin alignment through their thickness dominated by the interface exchange interaction. The dependence on the applied field, however, is the opposite of that in the GdN layers; the Sm spin alignment is in fact weaker in 6 T than in the remanent magnetisation. Again that follows from the exchange-Zeeman interaction conflict in the SmN layers; the remanent magnetisation in the GdN layer is enough to align the entire thickness of the SmN layers in zero field, but, as illustrated in Figure 3, the Zeeman interaction in an applied field reverses the spin alignment in the center of the SmN layers.

A similar system has been studied in NdN/GdN superlattices via XMCD and magnetisation measurements.[23] In that system the NdN shares the orbital-dominant magnetisation of SmN, but the net magnetisation is much larger than that of SmN at around 1 μ_B/Nd^{3+}. At the lowest temperatures of 5 K the NdN has such a large anisotropy energy that the NdN magnetisation remains rigid while an exchange spring forms in the GdN layer. This is in contrast to the current SmN/GdN system, with the difference arising primarily from the larger magnetisation and anisotropy energy in NdN compared to SmN. At higher temperatures near the Curie temperature of NdN, the NdN anisotropy energy becomes small, and XMCD measurements provided strong evidence of exchange spring formation within the NdN layers while the magnetisation of GdN layers was relatively bulk-like; the same situation as the current SmN/GdN superlattice. While the SmN/GdN and NdN/GdN systems share many features (notably the orbital moment dominant magnetisation), interpreting the various magnetic arrangements which arise in

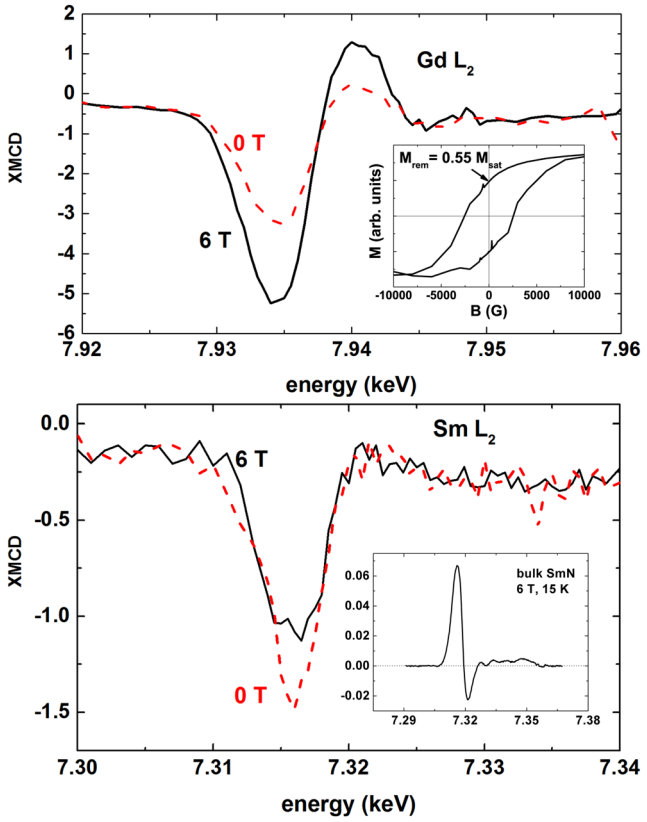

FIG. 2. (Colour online) L_2-edge XMCD in a 6×[10 nm GdN/16 nm SmN] superlattice at a temperature of 2 K. The magnetisation of the GdN layers was saturated in the 6 T field, so that the reduced Gd signal after returning the field to zero corresponds to the remanent magnetisation, as illustrated by the SQUID data shown in the inset of the upper panel. The contrasting increase of the Sm signal results from the absence of interface-exchange-vs.-Zeeman conflict because the Zeeman interaction is absent in zero field. The inset in the lower panel shows L_2-edge XMCD from bulk SmN (adapted from Ref. 10) for comparison, note the reversed sign.

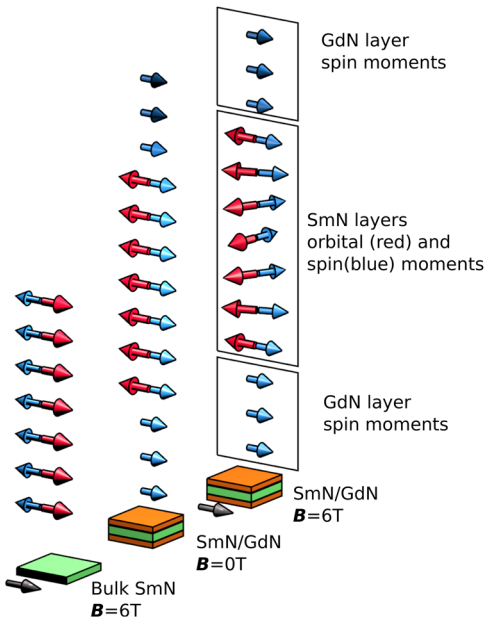

FIG. 3. (Colour online) A sketch of the magnetic alignments in a SmN film at 6 T and in the SmN/GdN superlattice in both 0 T and 6 T. In a SmN film, the magnetisation is uniformly aligned by the applied field, with the orbital moment (red) determining the net magnetisation direction, while the spin moment is antiparallel. In the superlattice, the GdN-SmN interface exchange energy dominates the SmN layer configuration at 0 T, resulting in a negative magnetisation of the SmN layer. The negative magnetisation of the SmN layers causes the sign reversal of the Sm XMCD signal in Fig. 2 as compared to the bulk. At 6 T the SmN magnetisation partially reverses due to the Zeeman interaction competing against the GdN-SmN interface exchange. The result is an exchange spring or twisted magnetisation in the SmN layer, resulting in a lower net magnetisation in 6 T, observed in a decrease of the XMCD signal in the Sm L_2 edge XMCD at 6 T (Fig. 2). Even at 6 T the average magnetisation of the SmN layers is still negative, which means the XMCD signal remains the opposite sign as compared to the bulk.

each system depends on understanding the relative balance of intra-layer exchange, interface exchange, anisotropy energy, and Zeeman energy for each.

B. Magneto-electronic transport

In contrast with the magnetic properties, electron transport in the LN is a strong function of electron doping as determined by the nitrogen-vacancy concentration. In the absence of any information about band offsets in the GdN/SmN superlattice system, it is not *a priori* certain whether electrons will reside in the GdN or SmN layers, or indeed be shared equally between them. We thus start by highlighting signatures of GdN and SmN transport in the temperature-dependent resistivity of a superlattice.

Figure 4 shows the temperature dependence of the average resistivity of the 6×[10 nm GdN/16 nm SmN] superlattice for which XMCD is reported above. A positive temperature coefficient of resistance at ambient temperature is as expected from the degenerate electron gas in these heavily doped films. As the temperature is lowered, there is a pair of resistance peaks near the Curie temperatures of GdN (60 K) and SmN (30 K). Such peaks are well understood; they arise from magnetic-disorder electron scattering that rises to a maximum at the transition temperatures.[24] The presence of both with very similar magnitudes in Figure 4 signals that current flows in both the GdN and SmN layers. Significantly the GdN peak is largely missing in a field of 5 T, as is commonly seen also in homogeneous GdN films.[25] It follows from the reduction of magnetic disorder driven by the strong Zeeman interaction. Such a reduced scattering is not found at the SmN peak as a result of a 200-fold weaker Zeeman interaction in the near-zero magnetisation of SmN. The dominance of magnetic disorder scattering is further supported by the inset in Figure 4, which shows the normalised magnetoresistance (MR = [R(B) - R(0)]/R(0)) at 20 and 60 K. The magnetoresistance is negative and largest near the GdN Curie temperature, where spin-disorder scattering is strongest. This behaviour is very similar to what was observed for GdN.[26] In the superlattice the magnetoresistance is much smaller than the ~20 % for single layer GdN,[26] as expected by the weaker magnetoresistance in SmN.

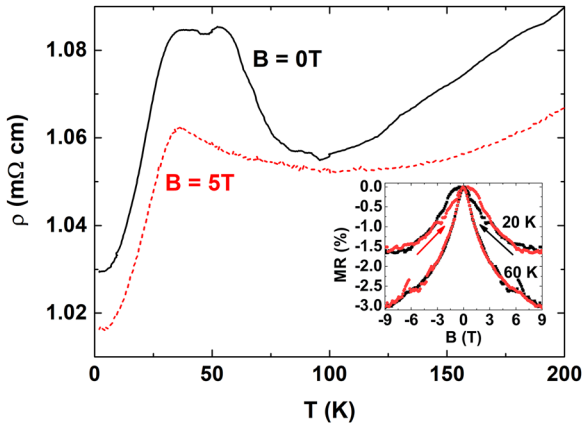

FIG. 4. (Colour online) Temperature-dependent average resistivity of the 6×[10 nm GdN/16 nm SmN] superlattice in zero magnetic field contrasted with its resistivity in 5 T. The overall behaviour is of a very heavily doped semiconductor harbouring a degenerate electron gas. The peak below 100 K results from spin-disorder scattering in the vicinity of the Curie temperatures in GdN (70 K) and SmN (30 K). The strong Zeeman interaction in GdN severely reduces spin-disorder scattering, thus removing the 70 K peak, but a two-orders-of-magnitude weaker Zeeman interaction in SmN severely limits the reduction of the 30 K peak. Inset: Magnetoresistance measured at 20 and 60 K in increasing and decreasing fields as marked by the arrows.

Low-temperature Hall effect data are presented in Figure 5. The ambient-temperature slope of 2.5 $\mu\Omega$cm/T (not shown) suggests an electron concentration of 2.5 $\times 10^{20}$ cm^{-3}, if one assumes carriers in only one band in a homogeneous material. However, the resistivity data already shown establishes conduction in both GdN and SmN layers, and in view that the carriers in doped SmN are proposed to reside in a heavy-fermion 4f band,[27] rather than the 5d-band conduction channel as in GdN, one must treat the carrier concentration as no more than an estimate. Nonetheless we note that cooling from 80 to 60 K, where GdN becomes ferromagnetic, the high-field slope representing the ordinary Hall effect is unchanged. On the other hand the slope reduces across the SmN Curie temperature (30 K), suggesting a two-fold increase in the carrier concentration that we have never seen in homogeneous SmN films. It is likely that the change in slope results from a changing balance between the 5d versus 4f conduction channels rather than an enhanced electron concentration.

The step across -2 to +2 T is the anomalous Hall effect, a result of the spin–orbit interaction on the mobile charge carriers that deflects the carriers in a direction that depends on their spin orientation. An accumulation of charge appears at the two sample edges *only* if there is a concentration imbalance between the spin-up vs. spin-down carriers. In the GdN that imbalance is complete, i.e., there is an electron current in only one spin channel,[28] until the carrier concentration reaches 10^{21} cm^{-3}. At lower electron doping the anomalous Hall effect is simply determined by the spin–orbit interaction in the conduction channel and the carrier concentration. The spin–orbit interaction of the GdN conduction channel leads to an anomalous Hall effect of ~ 2 $\mu\Omega$ cm, much smaller than seen here.[28] On the other hand the SmN 4f band has a spin–orbit interaction a factor of 10 larger than GdN,[19] in better agreement with the data of

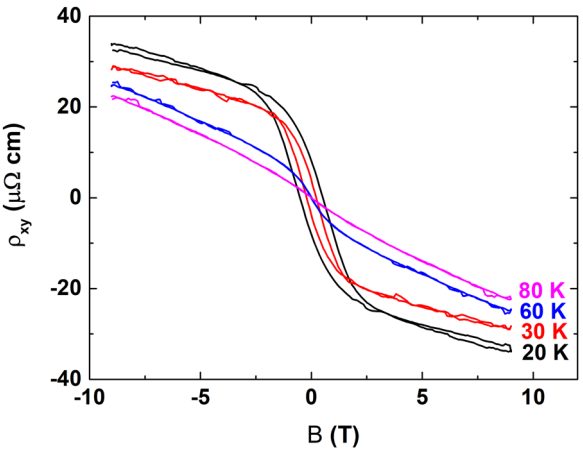

FIG. 5. (Colour online) The Hall resistivity of the 6×[10 nm GdN/16 nm SmN] superlattice shows a clear anomalous Hall effect in the ferromagnetic state as is discussed in the text.

Figure 5 suggesting that the anomalous Hall effect here is dominated by $4f$ electrons in SmN.

IV. SUMMARY AND CONCLUSIONS

GdN/SmN superlattices have been grown with varying SmN layer thickness and the magnetic and electrical transport properties have been investigated. Magnetisation measurements on the series of superlattices with varying SmN thickness show the magnetic response of isolated GdN layers for a SmN thickness of ≥ 5 nm, but that of a thicker GdN layer as the SmN thickness is reduced below that limit. XMCD measurements furthermore show that at zero applied field the spin alignment of the SmN layers is exchange coupled to the GdN. When a large field is applied to the sample the Zeeman interaction is then apparent in the SmN layers, which now aligns the $4f$ spin moment anti-parallel to the applied field. Electrical transport measurements show a response to magnetic ordering transitions in both GdN and SmN layers.

The results presented demonstrate that the varied spin/orbital behaviour observed in homogeneous LN samples can be translated through to multi-layer structures. Furthermore, the combination of materials with opposing spin and orbital magnetisations gives rise to complex magnetic properties which may be exploited in modern device structures.

ACKNOWLEDGMENTS

The research described in the present paper was supported by the New Zealand Marsden Fund (Grant No. 13-VUW1309). The MacDiarmid Institute is supported under the New Zealand Centres of Research Excellence Programme. This research used resources of the Advanced Photon Source, a U.S. Department of Energy (DOE) Office of Science User Facility operated for the DOE Office of Science by Argonne National Laboratory under Contract No. DE-AC02-06CH11357.

DATA AVAILABILITY

The data that support the findings of this study are available from the corresponding author upon reasonable request.

REFERENCES

[1] S. Stemmer and S. James Allen, Annu. Rev. Mater. Res. **44**, 151 (2014).
[2] S. Subramanian, Bull. Mater. Sci. **13**, 121–133 (1990).
[3] C. Weisbuch and J. Nagle, Phys. Scr. **T19A**, 209 (1987).
[4] B. Saha, A. Shakouri, and T. D. Sands, Appl. Phys. Rev. **5**, 021101 (2018).
[5] A. Fert, Rev. Mod. Phys. **80**, 1517 (2008).
[6] H. Kepa, J. Kutner-Pielaszek, J. Blinowski, A. Twardowski, C. F. Majkrzak, T. Story, P. Kacman, R. R. Gałazka, K. Ha, H. J. M. Swagten, W. J. M. de Jonge, A. Y. Sipatov, V. Volobuev, and T. M. Giebultowicz, Europhysics Letters (EPL) **56**, 54 (2001).
[7] F. Natali, B. J. Ruck, N. O. V. Plank, H. J. Trodahl, S. Granville, C. Meyer, and W. R. L. Lambrecht, Prog. Mater. Sci. **58**, 1316 (2013).
[8] S. Granville, B. J. Ruck, F. Budde, A. Koo, D. J. Pringle, F. Kuchler, A. R. H. Preston, D. H. Housden, N. Lund, A. Bittar, G. V. M. Williams, and H. J. Trodahl, Phys. Rev. B **73**, 235335 (2006).
[9] C. Meyer, B. J. Ruck, J. Zhong, S. Granville, A. R. H. Preston, G. V. M. Williams, and H. J. Trodahl, Phys. Rev. B **78**, 174406 (2008).
[10] E.-M. Anton, B. J. Ruck, C. Meyer, F. Natali, H. Warring, F. Wilhelm, A. Rogalev, V. N. Antonov, and H. J. Trodahl, Phys. Rev. B **87**, 134414 (2013).
[11] J. F. McNulty, E.-M. Anton, B. J. Ruck, F. Natali, H. Warring, F. Wilhelm, A. Rogalev, M. M. Soares, N. B. Brookes, and H. J. Trodahl, Phys. Rev. B **91**, 174426 (2015).
[12] F. Natali, B. J. Ruck, H. J. Trodahl, D. L. Binh, S. Vezian, B. Damilano, Y. Cordier, F. Semond, and C. Meyer, Phys. Rev. B **87**, 035202 (2013).
[13] F. Hulliger, *Handbook on the Physics and Chemistry of the Rare Earths* (North Holland, 1979), Vol. 4, pp. 153–236.
[14] K. Khazen, H. J. von Bardeleben, J. L. Cantin, A. Bittar, S. Granville, H. J. Trodahl, and B. J. Ruck, Phys. Rev. B **74**, 245330 (2006).
[15] P. Larson, W. R. L. Lambrecht, A. Chantis, and M. van Schilfgaarde, Phys. Rev. B **75**, 045114 (2007).
[16] H. J. Trodahl, A. R. H. Preston, J. Zhong, B. J. Ruck, N. M. Strickland, C. Mitra, and W. R. L. Lambrecht, Phys. Rev. B **76**, 085211 (2007).
[17] C.-M. Lee, H. Warring, S. Vézian, B. Damilano, S. Granville, M. Al Khalfioui, Y. Cordier, H. J. Trodahl, B. J. Ruck, and F. Natali, Appl. Phys. Lett. **106**, 022401 (2015).
[18] J. F. McNulty, B. J. Ruck, and H. J. Trodahl, Phys. Rev. B **93**, 054413 (2016).
[19] W. F. Holmes-Hewett, F. H. Ullstad, B. J. Ruck, F. Natali, and H. J. Trodahl, Phys. Rev. B **98**, 235201 (2018).
[20] F. Ullstad, G. Bioletti, J. R. Chan, A. Proust, C. Bodin, B. J. Ruck, J. Trodahl, and F. Natali, ACS Omega **4**, 5950 (2019).
[21] A. Shaib, F. Natali, J. R. Chan, F. Ullstad, W. F. Holmes-Hewett, J. D. Miller, B. J. Ruck, and H. J. Trodahl, Mater. Res. Express **7**, 046404 (2020).
[22] G. van der Laan and A. I. Figueroa, Coord. Chem. Rev. **277-278**, 95 (2014).
[23] J. F. McNulty, E.-M. Anton, B. J. Ruck, M. Suzuki, M. Mizumaki, and H. J. Trodahl, Phys. Rev. B **100**, 094441 (2019).
[24] T. Maity, H. J. Trodahl, F. Natali, B. J. Ruck, and S. Vézian, Phys. Rev. Materials **2**, 014405 (2018).
[25] F. Leuenberger, A. Parge, W. Felsch, K. Fauth, and M. Hessler, Phys. Rev. B **72**, 014427 (2005).
[26] T. Maity, H. J. Trodahl, S. Granville, S. Vézian, F. Natali, and B. J. Ruck, J. Appl. Phys. **128**, 213901 (2020).
[27] W. F. Holmes-Hewett, R. G. Buckley, B. J. Ruck, F. Natali, and H. J. Trodahl, Phys. Rev. B **99**, 205131 (2019).
[28] H. J. Trodahl, F. Natali, B. J. Ruck, and W. R. L. Lambrecht, Phys. Rev. B **96**, 115309 (2017).